Pharmaceutical Sciences and Drug Design
ISSN: 3062-4428
2026, Volume 6, Issue 1, Page No: 39-56

Available online at: www.galaxypub.co/page/journals

Galaxy Publication

Galaxy Publication

MAPK-Dependent Anticancer Effects of YK-4-279 in Osteosarcoma: Cell Cycle Arrest, DNA Damage, and Apoptosis

Lucas Meyer[1]*, Anna Schmid[2], Stefan Braun[1]

[1]Department of Pharmaceutical Innovation and Drug Design, Faculty of Science, ETH Zurich, Zurich, Switzerland.
[2]Department of Medicinal Chemistry and Drug Systems, Faculty of Medicine, University of Bern, Bern, Switzerland.

***E-mail** ✉ lucas.meyer@gmail.com

Received: 17 October 2025; **Revised:** 21 January 2026; **Accepted:** 26 January 2026

ABSTRACT

YK-4-279 is an emerging anticancer compound that has demonstrated activity across a range of tumor models. Osteosarcoma (OS), a highly aggressive bone malignancy predominantly diagnosed in adolescents, still lacks satisfactory therapeutic options. A detailed investigation of how YK-4-279 functions in OS is essential for determining its potential clinical relevance. Therefore, the present study aimed to evaluate its effects on OS cell viability, proliferation, DNA damage, cell cycle regulation, apoptosis, and MAPK signaling activity, potentially providing a novel basis for osteosarcoma treatment and prognosis. In vitro experimental systems were used to evaluate the effects of YK-4-279 on osteosarcoma cell viability, proliferation, programmed cell death, cell cycle distribution, and DNA damage responses. Its regulatory influence on MAPK signaling activity was also analyzed. To further verify pathway involvement, cells were treated with YK-4-279 in combination with a P38-specific inhibitor. Treatment with YK-4-279 significantly impaired osteosarcoma cell survival and proliferation, induced arrest at the G2/M checkpoint, and increased both apoptotic activity and DNA damage levels. In parallel, MAPK signaling was activated, as indicated by enhanced phosphorylation of ERK1/2, JNK, and P38 MAPK. Notably, inhibition of P38 partially mitigated these effects, supporting a functional role for MAPK signaling in mediating the compound's anticancer activity. YK-4-279 exerts strong inhibitory effects on osteosarcoma cell growth by promoting DNA damage, enforcing cell cycle arrest, and activating apoptosis through MAPK pathway stimulation. These findings suggest its potential as a promising candidate for osteosarcoma therapy.

Keywords: YK-4-279, Osteosarcoma, MAPK signaling pathway, Cell cycle, DNA damage, Apoptosis

How to Cite This Article: Meyer L, Schmid A, Braun S. MAPK-Dependent Anticancer Effects of YK-4-279 in Osteosarcoma: Cell Cycle Arrest, DNA Damage, and Apoptosis. Pharm Sci Drug Des. 2026;6(1):39-56. https://doi.org/10.51847/ZyReFZZLfR

Introduction

Osteosarcoma (OS) is a frequent and highly malignant primary bone cancer, with an estimated global incidence of approximately 3 cases per million people and representing 11.7% of all primary bone tumors [1]. It primarily affects children and adolescents and most commonly develops in the metaphyseal regions of long bones, including the distal femur, proximal tibia, and proximal humerus [2]. The disease is characterized by aggressive behavior and poor prognosis, with about 80%–90% of patients already harboring micrometastatic disease at diagnosis [3]. Although combined treatment strategies involving chemotherapy, surgery, and radiotherapy can raise 5-year survival rates to roughly 70%, outcomes remain poor for recurrent or metastatic cases, where survival drops to around 20% [4]. This creates considerable emotional stress for patients and imposes a heavy socioeconomic burden, while therapeutic progress in OS has largely stagnated in recent years [5]. Therefore, there is an urgent need for innovative treatment strategies that can improve survival outcomes and provide more effective clinical management options.

DNA damage, cell cycle arrest, and activation of programmed cell death represent effective approaches for selectively removing malignant cells [6]. These biological processes are also key targets in the development of new anticancer agents, where drugs that interact directly with DNA can suppress cell division and ultimately trigger cellular death [7]. The DNA damage response is initiated through the rapid detection of lesions by sensor proteins such as ATM and CHK, which subsequently activate downstream mediators involved in DNA repair pathways, including p21 and CDK [8–12]. In parallel, activation of this response results in inhibition of cell cycle progression and consequent cell cycle arrest [13]. When DNA damage is extensive and cannot be repaired, apoptotic signaling pathways are then activated [14]. Apoptosis is a tightly regulated form of programmed cell death in multicellular organisms that is essential for removing damaged or unnecessary cells in response to developmental cues, cellular stress, and irreparable genomic injury. Impairment of apoptotic mechanisms contributes to tumor development and progression [15].

At present, emerging therapeutic approaches such as targeted therapy [16] and nanotechnology-based treatment [17] are gaining attention. In cancer research, tumor cells have been shown to frequently overexpress specific molecular signatures that may arise from proto-oncogenes or components of normal signaling cascades. These molecules can be selectively targeted to inhibit their function, thereby suppressing tumor growth or inducing cancer cell death [18]. Compared with conventional chemotherapy, this strategy offers higher specificity and reduced systemic toxicity. A growing number of targeted agents have already been approved for first- and second-line treatment of different malignancies, demonstrating encouraging clinical outcomes [19–22]. Accordingly, molecular targeted therapy is widely recognized as a promising direction in cancer treatment.

The E26 transformation-specific (ETS) family comprises 28 transcription factors. ETS activity is controlled by multiple intracellular signaling cascades, including MAPK-related kinases (ERK, p38, and JNK). Dysregulation of this system is commonly associated with oncogenic transformation and tumor progression [23], including in Ewing's sarcoma (ES) [24–26], brain malignancies [27], hematological cancers [28, 29], and prostate cancer [30, 31]. Within this family, ETS variant 1 (ETV1) has been identified as an important regulator of metastatic progression in both Ewing's sarcoma and osteosarcoma (OS) [32, 33]. YK-4-279 is a small-molecule inhibitor targeting ETV1 and has shown significant antitumor effects in Ewing's sarcoma (ES) [34], prostate cancer [35], and neuroblastoma [36]. Mechanistically, YK-4-279 binds to EWS-FLI1 and prevents its interaction with DHX9, thereby inhibiting growth and inducing apoptosis in ES cells. It also suppresses ETS protein function by disrupting protein–protein interactions between ETS factors and their partners [37]. This mode of action, which interferes with specific protein interactions rather than broadly inhibiting essential enzymes, is considered to provide greater cancer selectivity [38]. However, the mechanistic role of YK-4-279 in osteosarcoma remains insufficiently characterized. Therefore, the present study aimed to evaluate its effects on OS cell viability, proliferation, DNA damage, cell cycle regulation, apoptosis, and MAPK signaling activity, potentially providing a novel basis for osteosarcoma treatment and prognosis.

Materials and Methods

Reagents and antibodies

YK-4-279 (Cat. No. Y10002; CAS: 1037184–44-3) was supplied by Beijing Psaitong Biotechnology Co., Ltd. This compound possesses the molecular formula C17H13Cl2NO4 and a molecular mass of 366.20 g/mol. Its physicochemical profile includes a density of 1.5 ± 0.1 g/cm3, a boiling temperature of 608.9 ± 55.0 °C at 760 mmHg, a melting interval of 149–151 °C, and a flash point of 322.1 ± 31.5 °C. For experimental procedures, a 50 mM stock solution was prepared in dimethyl sulfoxide (DMSO; Solarbio, Cat. No. D8371), aliquoted, and stored at −80 °C to maintain stability. The experimental reagents included CCK-8 (C0039, Beyotime), 0.1% Crystal Violet Staining Solution (G1063, Solarbio), DNA Content Quantification Kit for Cell Cycle Analysis (CA1510, Solarbio), Annexin V-FITC Apoptosis Detection Kit (BD PharmingenTM, 556547), Hoechst 33342/PI (Beyotime, P0137), and SB203580 (Psaitong Bio, S10108).

Primary antibodies used in this study were Phospho-ATM (Ser1981) (4526s, 1:1000), γ-H2AX (Ser139) (9718s, 1:1000), Phospho-ERK1/2 (Thr202/Tyr204) (4370s, 1:1000), Phospho-JNK (Thr183/Tyr185) (9255s, 1:1000), β-actin (Ms) (3700s, 1:1000), and GAPDH (Rb) (5147s, 1:1000), obtained from Cell Signaling Technology (Danvers, MA, USA). Additional antibodies included ATM (ET1606-20, 1:1000), Chk2 (ET1610-52, 1:1000), p27 (ET1608-61, 1:1000), Cyclin B1 (ET1608-27, 1:1000), and Cyclin D1 (ET1601-31, 1:1000), provided by HUABIO (China). Further antibodies comprised PARP1 (13371-1-AP, 1:500), Caspase 8 (13423-1-AP, 1:500),

ERK1/2 (16443-1-AP, 1:1000), JNK (66210-1-Ig, 1:2000), Phospho-CHEK2 (Thr68) (29012-1-AP, 1:1000), p21 (10355-1-AP, 1:1000), p38 MAPK (14064-1-AP, 1:1000), and Phospho-p38 MAPK (Thr180/Tyr182) (28796-1-AP, 1:1000), sourced from Proteintech (China). Secondary antibodies consisted of Goat Anti-Rabbit IgG H&L (HRP) (ab205718, Rb: 1:20000), Goat Anti-Mouse IgG H&L (HRP) (ab205719, Ms: 1:10000), Goat Anti-Rabbit IgG H&L (Alexa Fluor® 488) (ab150077, 1:500), and Goat Anti-Mouse IgG H&L (Alexa Fluor® 594) (ab150116, 1:500), obtained from Abcam (Cambridge, UK).

Cells and cell culture

Osteosarcoma cell lines HOS (ZQ0952) and MG63 (ZQ0403) were provided by Shanghai Zhong Qiao Xin Zhou Biotechnology Co., Ltd. Authentication of all cell lines was performed using Short Tandem Repeat (STR) profiling to ensure identity verification. Cells were cultured in Minimum Essential Medium (MEM) supplemented with Non-Essential Amino Acids (NEAA) (Pricella, PM150410), 10% fetal bovine serum (FBS) (Abwbio, AB-FBS0500), and 1% Penicillin-Streptomycin (P1400, Solarbio). Incubation was maintained at 37 °C in a humidified atmosphere containing 5% CO2, and culture medium was replaced every 2–3 days.

Cell viability assay

The cytotoxic effect of YK-4-279 on osteosarcoma cells was evaluated using the CCK-8 assay system. HOS and MG63 cells in the exponential growth phase were collected by centrifugation, counted, and seeded into 96-well plates at a density of 1×104 cells per 100 μL per well. Each concentration group included six replicate wells. After a 24-hour attachment period, cells were exposed to YK-4-279 at graded concentrations of 8×10−5, 6×10−5, 4×10−5, 2×10−5, 1×10−6, 1×10−7, and 1×10−8 mol/L. Cells were subsequently incubated for either 24 or 48 hours before viability assessment. Two hours before measurement, CCK-8 reagent was added to each well and incubated at 37 °C under light-protected conditions. Absorbance was measured at 450 nm, and viability was calculated using the formula: (OD of treated wells−OD of blank)/(OD of control wells−OD of blank). The half-maximal inhibitory concentration (IC50) of YK-4-279 was then determined.

Cell proliferation assay

The proliferative capacity of osteosarcoma (OS) cells following YK-4-279 exposure was evaluated using a colony formation assay based on Crystalline Violet staining. HOS and MG63 cells in the exponential growth phase were plated at a density of 1000 cells per well in 6-well culture plates and incubated overnight to allow cell attachment. Cells were then treated with YK-4-279 at final concentrations of 0, 1, and 5 μM, with culture medium exchanged every 2–3 days to maintain treatment conditions. After 14 days of incubation, culture media were removed, and cells were rinsed twice with ice-cold PBS to eliminate residual medium. Fixation was performed with 4% paraformaldehyde (PFA) for 30 minutes, followed by fixation removal. Cells were subsequently washed once with cold PBS and stained with 0.1% Crystalline Violet Staining Solution (G1063, Solarbio) for 10 minutes. Excess dye was removed by PBS washing, and plates were air-dried. Colony formation was then documented through imaging, and the number of visible colonies was quantified.

Cell cycle analysis

Flow cytometric analysis with propidium iodide (PI) staining was performed to determine the effect of YK-4-279 on cell cycle progression in OS cells. HOS and MG63 cells in logarithmic growth phase were seeded into 6-well plates and exposed to YK-4-279 at concentrations of 0, 5, and 10 μM for 24 hours. Cells were collected from each treatment group into flow cytometry tubes, washed once with PBS, and centrifuged. The resulting cell suspensions were adjusted to a density of 106 cells/mL, and 1 mL of single-cell suspension was prepared per sample.

Cells were fixed by adding 500 μL of pre-chilled 70% ethanol and incubating at 4 °C overnight to preserve cellular structure. After fixation, samples were washed with PBS before staining. RNase A (100 μL) was added to each pellet, followed by resuspension and incubation at 37 °C for 30 minutes in a water bath to remove RNA contamination. Subsequently, 400 μL of PI solution was introduced and gently mixed. Cells were incubated for 30 minutes at 4 °C in the dark to ensure proper staining and then analyzed by flow cytometry.

Immunofluorescence analysis

DNA double-strand breaks (DSBs) were assessed by detecting phosphorylated histone H2AX (γ-H2AX), a marker of DNA damage induced by YK-4-279 in OS cells. HOS and MG63 cells were seeded at 5 × 10 ^5 cells/mL onto

glass coverslips in 24-well plates and treated with 5 μM YK-4-279 for 24 hours. After treatment, cells were rinsed with PBS and fixed using 4% paraformaldehyde for 30 minutes. Membrane permeabilization was then performed with 0.1% Triton X-100 (Beyotime, P0096) for 30 minutes, followed by blocking with 5% BSA at 4 °C for 1 hour to prevent nonspecific antibody binding.

Cells were incubated overnight at 4 °C with primary antibodies targeting rabbit γ-H2AX (Ser139, 9718S, 1:100, green) and mouse α-Tubulin (66031-1-Ig, 1:100, red). After removal of unbound antibodies via PBS washing, cells were incubated with fluorescent secondary antibodies—Goat anti-Rabbit IgG H&L (Alexa Fluor® 488, ab150077, 1:500) and Goat anti-Mouse IgG H&L (Alexa Fluor® 594, ab150116, 1:500)—for 1 hour at room temperature.

Following secondary antibody incubation, cells were further processed at room temperature for 1 hour. Nuclei were then counterstained using DAPI-containing antifade mounting medium (Beyotime, P0131). Finally, fluorescence microscopy was used to visualize and analyze intracellular fluorescent signal distribution and intensity.

Hoechst33342/PI analysis

To determine whether YK-4-279 induces osteosarcoma (OS) cell death, a dual fluorescent staining approach using Hoechst 33342 and propidium iodide (PI) (Beyotime, P0137) was applied. HOS and MG63 cells were seeded onto coverslips in 24-well plates at a density of 100,000 cells/mL and exposed to 5 μM YK-4-279 for 24 hours. After treatment, Hoechst 33342 and PI were simultaneously applied, followed by incubation at 4 °C for 15 minutes. Cells were then rinsed with PBS to remove excess dye. Co-staining patterns, where Hoechst 33342 (blue) and PI (red) signals overlapped, were interpreted as indicators of cell death. Fluorescence microscopy was used for image acquisition and analysis.

Cell apoptosis analysis

Apoptosis induction by YK-4-279 in OS cells was evaluated by flow cytometry. The Annexin V-FITC Apoptosis Detection Kit (BD Pharmingen, 556547) was used according to protocol. HOS and MG63 cells in exponential growth were collected, counted, and adjusted to 1 × 106 cells/mL. Cells were plated into 6-well plates and treated with YK-4-279 at 0, 5, and 10 μM for 24 hours. Following treatment, adherent cells were detached using 0.25% trypsin without EDTA, while suspended cells were recovered by centrifugation at room temperature for 5–10 minutes. Cells were washed with ice-cold PBS and resuspended in 300 μL of 1× binding buffer. Subsequently, 5 μL Annexin V-FITC and 5 μL PI were added, gently mixed, and incubated for 15 minutes at room temperature in the dark. Before measurement, 200 μL of 1× binding buffer was added, and samples were analyzed using a CytoFLEX SRT flow cytometer (BECKMAN COULTER, BF17071).

Western blot analysis

Protein expression analysis was performed in HOS and MG63 cells. After PBS washing, cells were collected and lysed using RIPA buffer (Beyotime, P0013) supplemented with protease and phosphatase inhibitors. Lysis was carried out on ice for 30 minutes to ensure efficient protein extraction. Total protein concentration was measured using a BCA assay kit (Beyotime, P0010). Equal amounts of protein (30 μg per sample) were separated on 10% SDS-PAGE gels and transferred onto PVDF membranes.

Membranes were blocked using 5% non-fat dry milk (BD Difco™ Skim Milk, 232100), prepared by dissolving 0.5 g milk powder in 10 mL of 1× TBST containing 0.1% Tween 20. Blocking was performed at room temperature for 1 hour under gentle agitation.

After blocking, membranes were incubated overnight at 4 °C with a panel of primary antibodies including γ-H2AX (Ser139) (9718s, Rb, 1:1000), ATM (ET1606-20, Rb, 1:1000), Phospho-ATM (Ser1981) (4526s, Ms, 1:1000), Chk2 (ET1610-52, Rb, 1:1000), Phospho-CHEK2 (Thr68) (29012-1-AP, Rb, 1:1000), p21 (10355-1-AP, Rb, 1:1000), p27 (ET1608-61, Rb, 1:1000), Cyclin B1 (ET1608-27, Rb, 1:1000), Cyclin D1 (ET1601-31, Rb, 1:1000), PARP1 (13371-1-AP, Rb, 1:500), Caspase 8 (13423-1-AP, Rb, 1:500), ERK1/2 (16443-1-AP, Rb, 1:1000), Phospho-p44/42 MAPK (ERK1/2) (Thr202/Tyr204) (4370s, Rb, 1:1000), JNK (66210-1-Ig, Ms, 1:2000), Phospho-SAPK/JNK (Thr183/Tyr185) (9255s, Ms, 1:1000), p38 MAPK (14064-1-AP, Rb, 1:1000), Phospho-p38 MAPK (Thr180/Tyr182) (28796-1-AP, Rb, 1:1000), β-actin (3700s, Ms, 1:1000), and GAPDH (5147s, Rb, 1:1000).

Membranes were then washed with 1× TBST and incubated with HRP-conjugated secondary antibodies at room temperature for 1 hour. The secondary antibodies used were Goat Anti-Rabbit IgG H&L (HRP) (ab205718, Rb, 1:20000) and Goat Anti-Mouse IgG H&L (HRP) (ab205719, Ms, 1:10000). After incubation, membranes were washed three times with 1× TBST to remove unbound antibodies.
Detection was performed using an enhanced chemiluminescence (ECL) system, and protein band intensities were quantified. Relative expression levels were calculated by normalizing target protein signals to internal loading controls.

Animal study
Female BALB/c-nu nude mice (SPF grade, approximately 15 g, 5–6 weeks old; Certificate No. 37072610100546123) were obtained from Jinan Pengyue Experimental Animal Breeding Co., Ltd. (License No. SCXK [Lu] 20220006). Animals were maintained under strict SPF barrier conditions, with environmental control set at 22 ± 2 °C temperature, 50%–60% relative humidity, and a 12-hour light/dark cycle, while receiving food and water ad libitum. After a one-week acclimation period, mice (n = 12) were inoculated subcutaneously in the right axilla with 1 × 107 MG63 cells suspended in 200 µL of a 1:1 Matrigel/PBS mixture. The mice were then randomly allocated into two groups: a vehicle control group (PBS) and a treatment group receiving YK-4-279 at 30 mg/kg/day. All administrations were performed via intraperitoneal injection, and animals were monitored throughout the experiment. Tumor growth was measured every 3 days, and tumor volume was estimated using the formula: Volume = (L × S^2) × 0.5, where L represents the maximum diameter and S the minimum diameter. After 28 days, mice were anesthetized and sacrificed; tumors were excised, weighed, and preserved for further analyses.

Statistical analysis
Each experiment was performed at least 5 times independently, and data are presented as mean ± standard deviation (SD). Statistical comparisons between two groups were conducted using a two-tailed paired Student's t-test. For datasets involving multiple groups, one-way analysis of variance (ANOVA) followed by Dunnett's post hoc test was applied using GraphPad Prism 9.0 when applicable. A P-value below 0.05 was considered statistically significant.

Results and Discussion

YK-4-279 significantly inhibits the growth of OS cells
The cytotoxic activity of YK-4-279 against osteosarcoma cell lines HOS and MG63 was assessed using the CCK-8 assay. Following 24 and 48 hours of exposure, a pronounced decrease in cell viability was observed in both lines across a concentration range of 80, 60, 40, 20, 1, 0.1, and 0.01 µM, demonstrating a clear dose-responsive pattern. The IC50 values were calculated as 2.41 ± 0.94 µM and 9.69 ± 3.96 µM for HOS cells at 24 and 48 hours, respectively, while MG63 cells exhibited IC50 values of 3.01 ± 0.72 µM and 0.92 ± 0.32 µM over the same time points **(Figures 1a and 1b).**

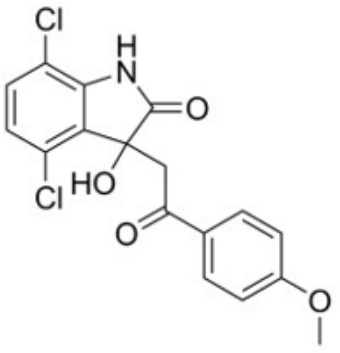

a)

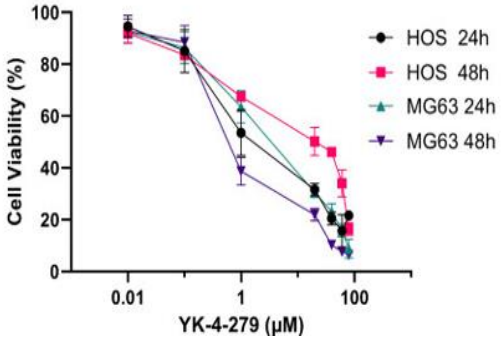

b)

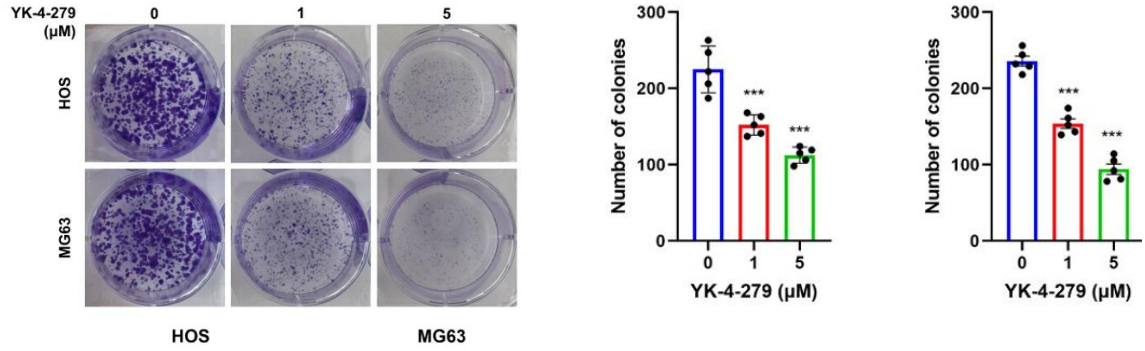

c) d)

Figure 1. YK-4-279 significantly inhibits the growth of OS cells: (a) Chemical structure of YK-4-279 (CAS No.: 1,037,184–44-3), (b) HOS and MG63 cells were treated with graded concentrations of YK-4-279 for 24 and 48 hours, and cell viability as well as IC50 values were determined using the CCK-8 assay, (c) The effect of YK-4-279 (0, 1, 5 μM) on clonogenic survival of HOS and MG63 cells was examined by colony formation assay. Colonies were fixed, stained with 0.1% crystalline violet solution, and quantified, and (d) Statistical evaluation of colony formation capacity. Experiments were conducted in five biological replicates per group, and data are shown as mean ± SD. ***P < 0.001.

To assess potential toxicity in non-cancerous cells, osteoblast MC3T3-E1 cells and rat renal podocytes were treated with a range of YK-4-279 concentrations (80, 60, 40, 20, 1, 0.1, and 0.01 μM). After 24 hours, the IC50 values were 10.63 ± 4.95 μM for MC3T3-E1 cells and 14.47 ± 6.94 μM for renal podocytes, indicating that normal cells are less sensitive to YK-4-279 than cancer cells.

The anti-proliferative effect of YK-4-279 was further validated through colony formation analysis. HOS and MG63 cells treated with 0, 1, and 5 μM YK-4-279 for 24 hours showed a marked, concentration-dependent decline in both colony number and size. Overall, these findings indicate that YK-4-279 effectively suppresses the viability and proliferative potential of osteosarcoma cells **(Figures 1c and 1d).**

YK-4-279 induces cell cycle arrest at the G2/M phase in OS cells

Inhibition of cell proliferation is closely associated with disruption of normal cell cycle progression [39]. To clarify whether YK-4-279 affects cell cycle distribution, flow cytometry was performed to analyze phase-specific changes. As illustrated in **Figures 2a and 2b**, treatment of HOS and MG63 cells with YK-4-279 at 0, 5, and 10 μM for 24 hours resulted in a clear shift in cell cycle distribution. Specifically, the fraction of cells in the G0/G1 phase was significantly reduced compared with untreated controls, while a marked accumulation of cells in the G2/M phase was observed. In addition, the proportion of S-phase cells also decreased following treatment in both cell lines. These results collectively indicate that YK-4-279 arrests OS cells primarily at the G2/M checkpoint.

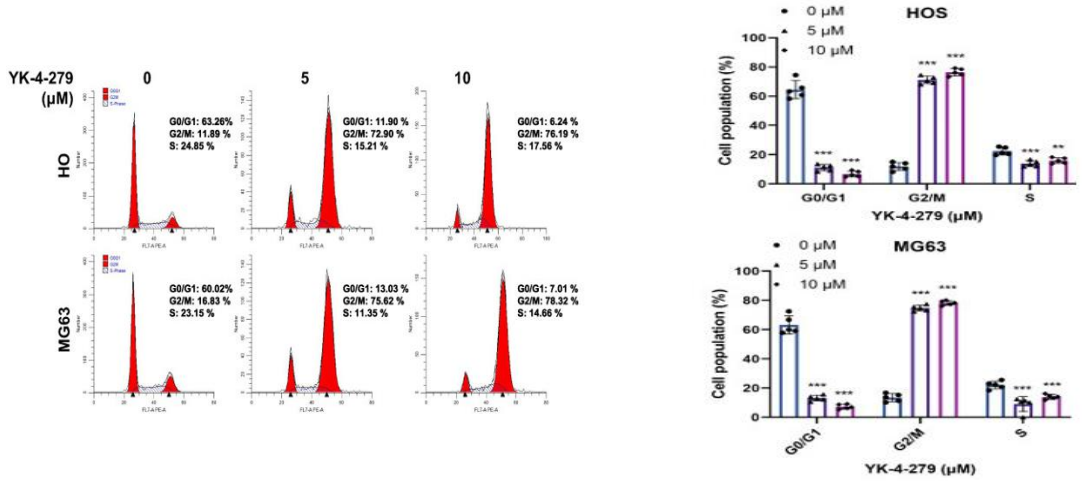

a) b)

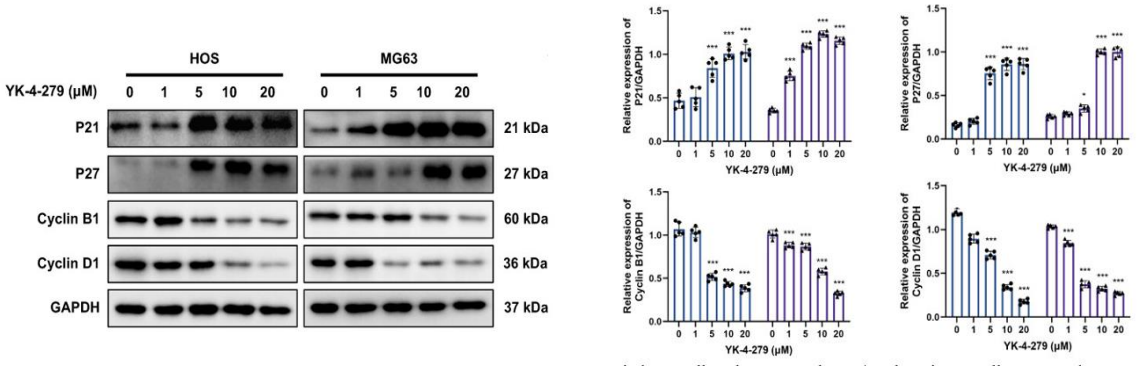

c) d)

Figure 2. YK-4-279 induces cell cycle arrest at the G2/M phase in OS cells. HOS and MG63 cells were treated with YK-4-279 (0, 1, 5, 10, 20 μM in Western blot, 0, 5 μM in flow cytometry) for 24 h: (a) Flow cytometric analysis and quantification of cell cycle distribution (G0/G1, S, and G2/M phases) in HOS and MG63 cells, (b) Statistical evaluation of cell cycle phase distribution in HOS and MG63 cells, (c) Western blot analysis of P21, P27, Cyclin B1, and Cyclin D1 expression, with GAPDH as a loading control, and (d) Quantitative analysis of protein expression levels of P21, P27, Cyclin B1, and Cyclin D1 in HOS and MG63 cells (●: HOS; ▲: MG63). Experiments were repeated five times, and results are expressed as mean ± SD. *P < 0.05, **P < 0.01, ***P < 0.001.

Cell cycle progression is tightly regulated by cyclin-dependent kinase inhibitors such as p21 and p27, which act as suppressors of cell cycle advancement, whereas Cyclin B1 and Cyclin D1 facilitate transition into the G2/M phase. To investigate whether these regulatory proteins are affected by YK-4-279, their expression levels were examined by Western blot. The results demonstrated that YK-4-279 markedly upregulated p21 and p27 expression, while simultaneously suppressing Cyclin B1 and Cyclin D1 levels in both HOS and MG63 cells **(Figures 2c and 2d).** These changes suggest that YK-4-279 impedes OS cell proliferation by reinforcing G2/M phase arrest through coordinated regulation of cell cycle proteins.

YK-4-279 triggered significant DNA damage via DNA damage sensor kinases in OS cells

The phosphorylated form of histone H2AX (γ-H2AX) is widely recognized as a sensitive biomarker of DNA double-strand breaks (DSBs) [40]. To evaluate whether YK-4-279 induces DNA damage, γ-H2AX expression was first assessed following treatment. Western blot analysis after 24 hours of exposure showed a pronounced increase in γ-H2AX protein levels in both HOS and MG63 cells **(Figures 3a and 3b).**

This finding was further supported by immunofluorescence analysis, which revealed strong nuclear accumulation of γ-H2AX (green signal) in YK-4-279–treated cells compared with controls **(Figures 3c and 3d).** Together, these results confirm that YK-4-279 significantly elevates DNA damage in a concentration-dependent manner.

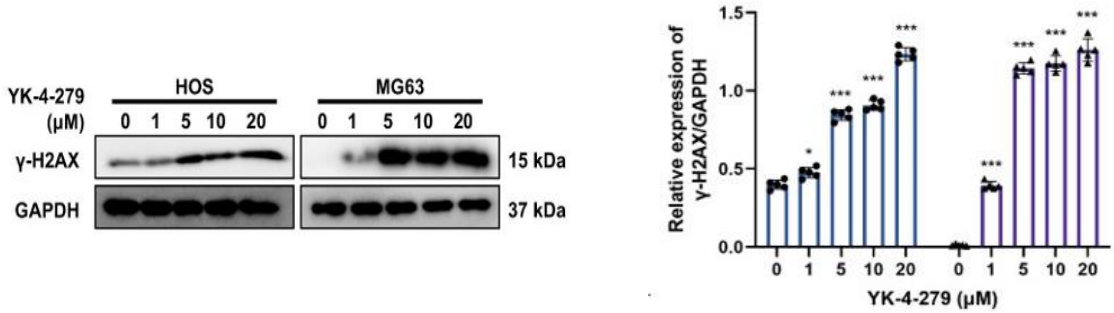

a) b)

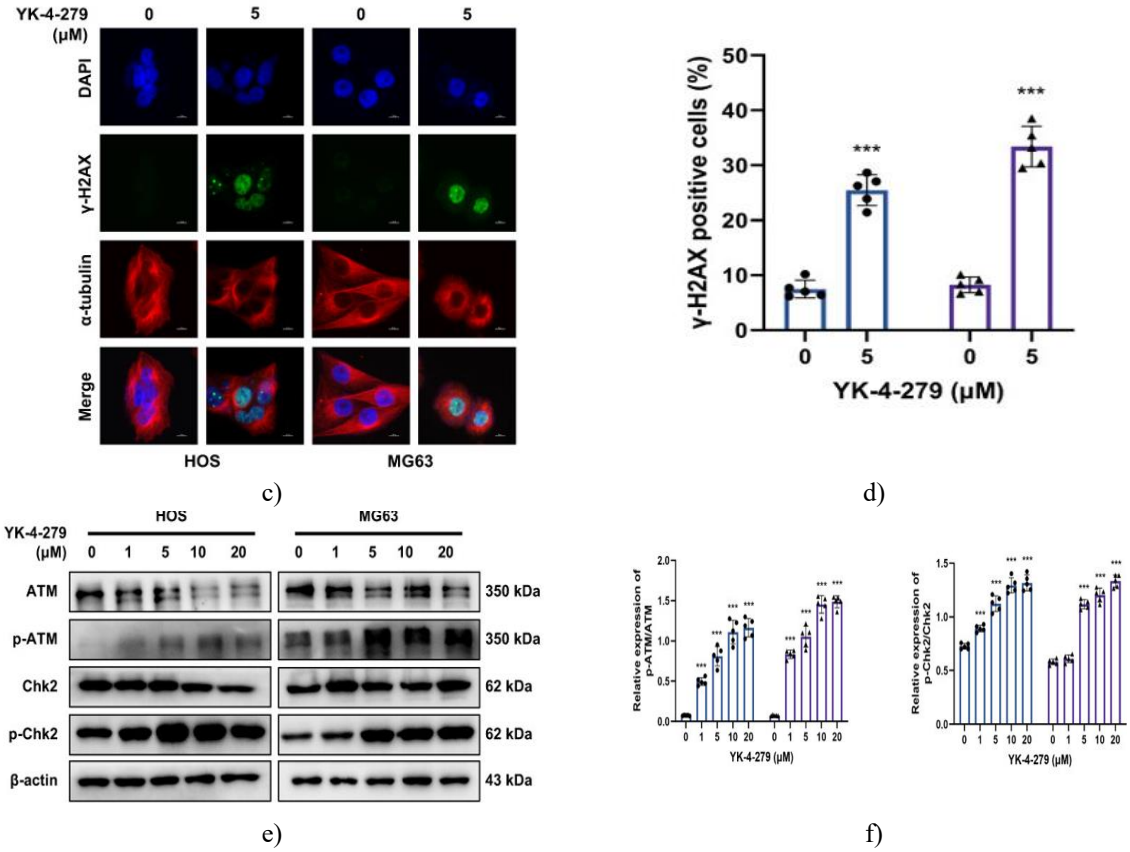

Figure 3. YK-4-279 triggered significant DNA damage via DNA damage sensor kinases in OS cells. HOS and MG63 cells were treated with YK-4-279 (0, 1, 5, 10, 20 μM in Western blot, 0, 5 μM in immunofluorescence) for 24 h: (a) Western blot analysis of γ-H2AX expression in HOS and MG63 cells, with GAPDH as a loading control, (b) Quantification of γ-H2AX protein levels in HOS and MG63 cells, (c) Immunofluorescence detection of γ-H2AX localization following YK-4-279 treatment. Scale bar = 10 μm, (d) Quantitative analysis of γ-H2AX fluorescence intensity per nucleus in HOS and MG63 cells, (e) Western blot analysis of ATM, p-ATM, Chk2, and p-Chk2 expression, with β-actin as a loading control, and (f) Quantitative evaluation of ATM, p-ATM, Chk2, and p-Chk2 levels in HOS and MG63 cells (●: HOS; ▲: MG63). Experiments were performed independently 5 times, and data are presented as mean ± SD. *P < 0.05, ***P < 0.001.

To further explore upstream signaling events in this DNA damage response, ATM and Chk2 activation were examined. Western blot analysis demonstrated that YK-4-279 significantly enhanced phosphorylation of both ATM and Chk2 in a dose-dependent manner in HOS and MG63 cells **(Figures 3e and 3f).** These results indicate that YK-4-279 activates DNA damage response signaling cascades, thereby impairing the viability and proliferation of osteosarcoma cells.

YK-4-279 triggers apoptosis in OS cells

Excessive DNA damage that exceeds the cellular repair capacity often leads to programmed cell death [41]. To evaluate whether YK-4-279 is capable of inducing osteosarcoma (OS) cell death, Hoechst 33342/PI dual staining was performed. Following 24 hours of exposure to 5 μM YK-4-279, strong red fluorescence signals were detected in the nuclei of both HOS and MG63 cells, indicating loss of membrane integrity and increased cell death. These observations confirmed that YK-4-279 markedly promotes cell death in OS cells **(Figures 4a and 4b).**

To further verify apoptotic induction, Annexin V-FITC/PI staining was performed and analyzed by flow cytometry. The results demonstrated a dose-dependent elevation in apoptotic cell populations in both HOS and MG63 cells after treatment with 5 μM and 10 μM YK-4-279. This confirmed that YK-4-279 effectively induces apoptosis in OS cells **(Figures 4c and 4d).**

Subsequently, apoptosis-associated proteins were examined by Western blot, focusing on PARP1 and Caspase 8 activation. The data showed a concentration-dependent increase in cleaved PARP1 and cleaved Caspase 8 levels

following YK-4-279 exposure **(Figures 4e and 4f).** Together, these findings indicate that YK-4-279 exerts cytotoxic effects in HOS and MG63 cells primarily by activating apoptotic pathways.

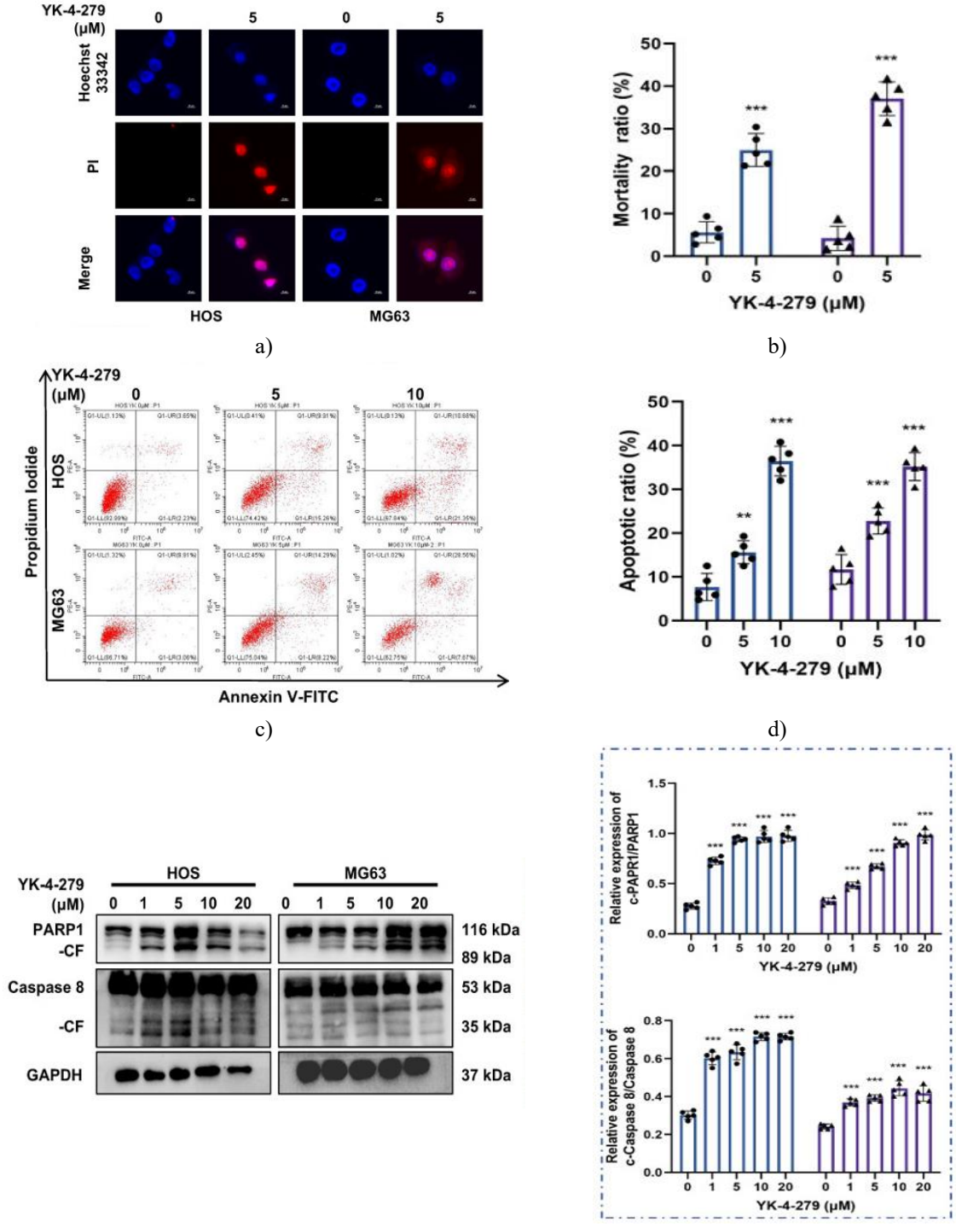

Figure 4. YK-4-279 triggers apoptosis in OS cells. HOS and MG63 cells were treated with YK-4-279 (0, 5 μM in immunofluorescence, 0, 5, 10 μM in flow cytometry, 0, 1, 5, 10, 20 μM in Western blot) for 24 h: (a) Assessment of cell death using Hoechst 33342/PI staining in HOS and MG63 cells. Scale bar = 10 μm, (b) Quantification of cell death–positive cells in HOS and MG63 populations, (c) Flow cytometric analysis of apoptosis using Annexin V-FITC/PI staining, (d) Quantitative analysis of apoptotic rates in HOS and MG63 cells, (e) Western blot detection of PARP1 and Caspase 8 expression, with GAPDH as the loading control, and (f) Densitometric analysis of PARP1 and Caspase 8 expression in HOS and MG63 cells (●: HOS; ▲:

MG63). Experiments were independently repeated five times, and data are expressed as mean ± SD. **P < 0.01, ***P < 0.001.

YK-4-279 induces activation of MAPK pathways in OS cells

After establishing that YK-4-279 induces DNA damage, G2/M arrest, and apoptosis in osteosarcoma cells, we next sought to identify the upstream signaling network that coordinates these biological effects. Considering that the MAPK cascade—particularly the stress-responsive p38 and JNK branches—plays a central role in linking DNA damage responses to cell cycle control and apoptosis regulation [42, 43], we hypothesized that MAPK signaling may act as a key mediator of YK-4-279 activity.

To test this, we examined whether YK-4-279 modulates MAPK pathway activation by assessing phosphorylation levels of ERK1/2, JNK, and p38 MAPK in HOS and MG63 cells. Western blot results showed that YK-4-279 treatment induced a dose-dependent increase in phosphorylation of ERK1/2, JNK, and p38 MAPK in both cell lines **(Figures 5a and 5b).** This early activation pattern suggests rapid engagement of MAPK signaling following drug exposure and provides mechanistic evidence supporting downstream functional effects. Overall, these findings demonstrate that YK-4-279 activates MAPK signaling in osteosarcoma cells.

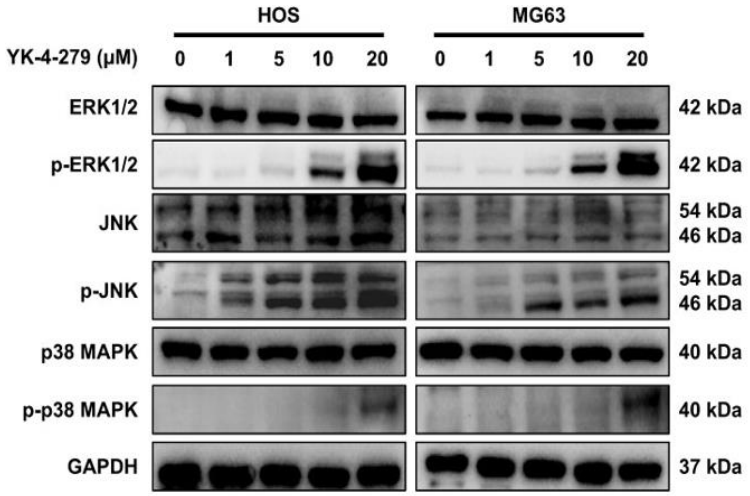

a)

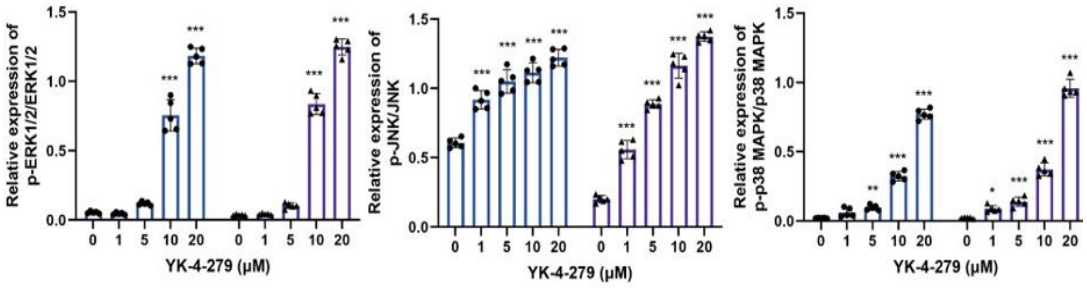

b)

Figure 5. YK-4-279 induces activation of MAPK pathways in OS cells: (a and b) Expression and phosphorylation levels of ERK1/2, JNK, and p38 MAPK were evaluated in HOS and MG63 cells treated with YK-4-279 (0, 1, 5, 10, and 20 μM) for 24 hours using Western blot analysis. Quantitative data were analyzed (●: HOS; ▲: MG63). Experiments were independently repeated five times, and results are presented as mean ± SD. *P < 0.05, **P < 0.01, ***P < 0.001.

Inhibiting MAPK pathways attenuates YK-4-279 cytotoxic activity on OS cells

To clarify whether the biological effects of YK-4-279—including reduced viability, DNA damage induction, and apoptosis—are mediated through MAPK signaling activation, HOS and MG63 cells were treated with YK-4-279 alone or in combination with SB203580, a p38 MAPK inhibitor.

First, DNA damage levels were evaluated using fluorescence-based detection of γ-H2AX. As illustrated in **Figures 6a and 6b**, co-treatment with SB203580 markedly reduced γ-H2AX fluorescence intensity compared with YK-4-279 monotherapy. This indicates that inhibition of p38 MAPK suppresses YK-4-279–induced DNA damage, supporting the involvement of MAPK signaling in this process.

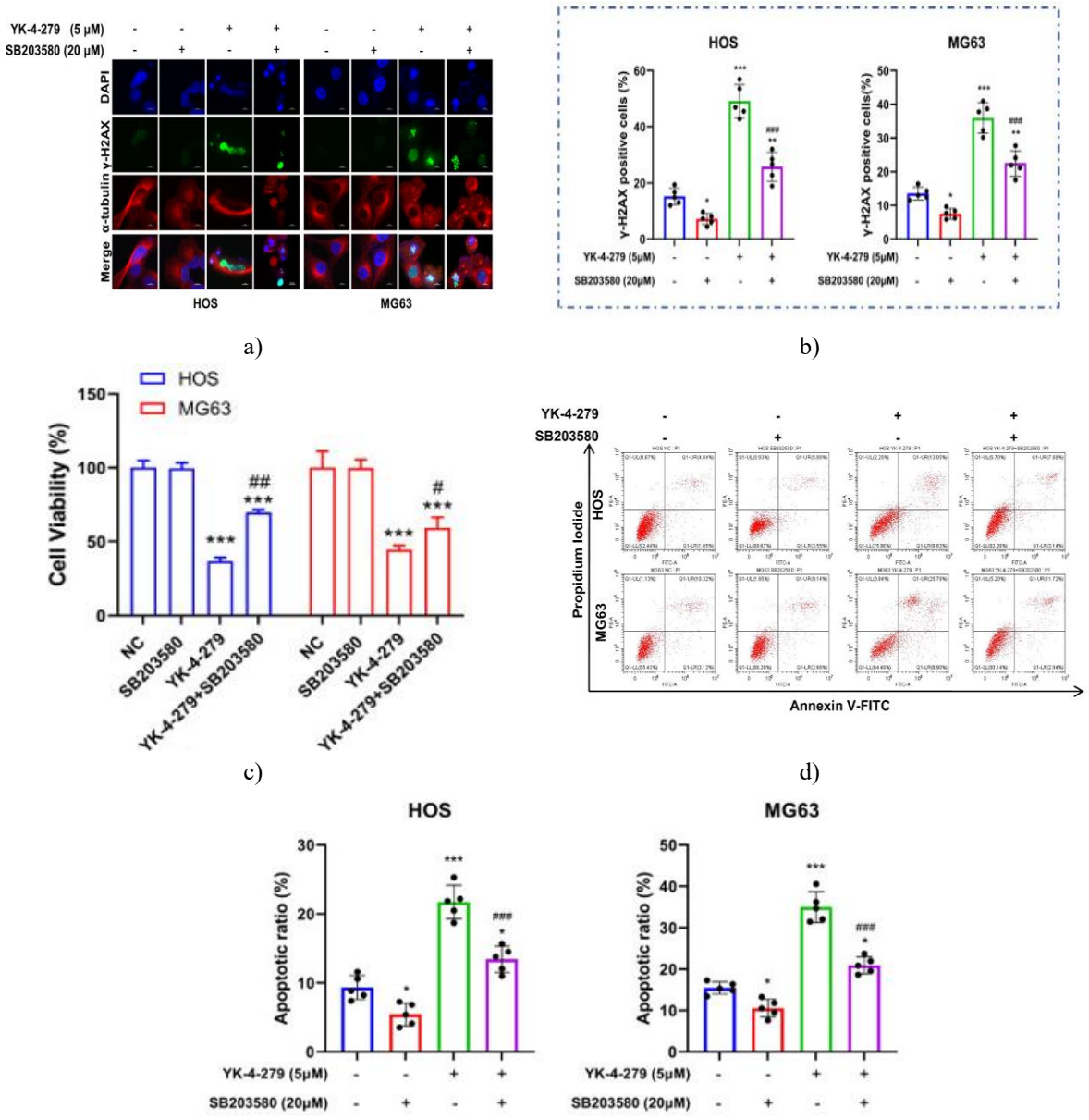

Figure 6. Inhibiting MAPK pathways attenuates YK-4-279 cytotoxic activity on OS cells. HOS and MG63 cells were treated with YK-4-279 and SB203580 (p38 MAPK inhibitor) for 24 hours: (a and b) Immunofluorescence analysis of γ-H2AX foci changes after treatment in HOS and MG63 cells, followed by quantitative evaluation, (c) Cell viability was measured using the CCK-8 assay in HOS and MG63 cells and statistically analyzed, (d and e) Apoptosis was assessed using Annexin V-FITC/PI staining and flow cytometry in HOS and MG63 cells, followed by quantitative analysis. Experiments were performed in five biological replicates per group, and data are shown as mean ± SD. *P < 0.05, **P < 0.01, ***P < 0.001: drug treatment group vs control. #P < 0.05, ##P < 0.01, ###P < 0.001: co-treatment group vs YK-4-279.

Next, cell viability was evaluated using the CCK-8 assay. YK-4-279 alone significantly decreased viability in both HOS and MG63 cells; however, when SB203580 was added, this inhibitory effect was partially reversed,

leading to increased cell viability compared with YK-4-279 treatment alone **(Figure 6c).** These findings indicate that MAPK pathway activation is required for the full cytotoxic effect of YK-4-279.

Subsequently, apoptotic changes were analyzed via flow cytometry. In both HOS and MG63 cells, YK-4-279 treatment led to a clear increase in apoptotic populations, whereas co-treatment with SB203580 significantly reduced apoptosis levels in both cell lines **(Figures 6d and 6e).**

Finally, protein expression was examined by Western blot, focusing on p-p38 MAPK, PARP1, and γ-H2AX. The results demonstrated that SB203580 co-treatment substantially decreased phosphorylation of p38 MAPK as well as levels of cleaved PARP1 and γ-H2AX compared with YK-4-279 alone in both HOS and MG63 cells **(Figures 7a and 7b).**

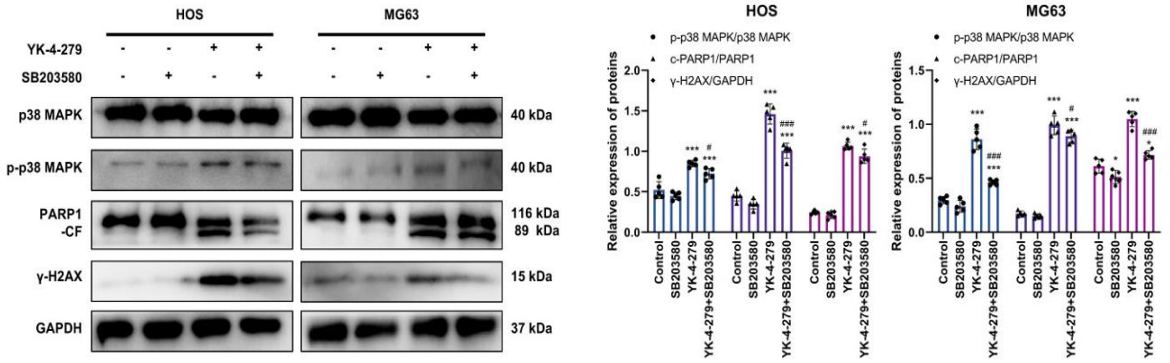

a) b)

Figure 7. Inhibition of the MAPK pathway attenuates YK-4-279-induced apoptosis and alterations in DNA damage-related proteins in OS cells. HOS and MG63 cells were treated with YK-4-279 and SB203580 (p38 MAPK inhibitor) for 24 hours: (a) Western blot analysis of p38 MAPK, p-p38 MAPK, PARP1, and γ-H2AX expression in HOS and MG63 cells, with GAPDH as the internal control, and (b) Quantitative evaluation of protein expression levels of p38 MAPK, p-p38 MAPK, PARP1, and γ-H2AX. Experiments were independently repeated five times, and data are presented as mean ± SD. *P < 0.05, ***P < 0.001: drug treatment group vs control. #P < 0.05, ###P < 0.001: co-treatment group vs YK-4-279.

Overall, these results demonstrate that the cytotoxic effects of YK-4-279—including suppression of viability, induction of DNA damage, and promotion of apoptosis—are largely dependent on activation of the MAPK signaling pathway.

YK-4-279 inhibits tumor growth in nude mice

To investigate the in vivo antitumor activity of YK-4-279 against osteosarcoma, MG63 cells were injected subcutaneously into nude mice, which were subsequently administered either PBS (control) or YK-4-279 at a dose of 30 mg/kg/day. Tumor dimensions were recorded every three days to construct growth curves. Importantly, YK-4-279 administration was well tolerated, with no noticeable adverse effects, such as reduced activity or weight loss, observed in treated mice. After 28 days of treatment, animals were euthanized, and tumors were excised and weighed.

Compared with the control group, YK-4-279 treatment significantly suppressed tumor progression. Molecular analysis by Western blot showed increased γ-H2AX expression, enhanced PARP1 cleavage, and elevated p-p38 MAPK levels following YK-4-279 administration, indicating activation of DNA damage and MAPK-related apoptotic signaling in vivo.

In addition, serum biochemical profiling revealed no significant differences in liver or kidney function parameters between treated and control groups, suggesting minimal systemic toxicity at the administered dose.

Overall, these findings demonstrate that YK-4-279 effectively suppresses osteosarcoma tumor growth in vivo while maintaining a favorable safety profile at therapeutic concentrations.

In this study, YK-4-279 was shown to exert broad antitumor effects in osteosarcoma (OS) models, including suppression of cell viability and proliferation, induction of DNA damage, disruption of cell cycle progression, and activation of apoptotic signaling. Importantly, these biological effects were accompanied by robust activation of the MAPK signaling cascade in OS cells. Taken together, these findings suggest that the anti-proliferative, pro-

damage, and pro-apoptotic actions of YK-4-279 are likely linked to MAPK pathway stimulation. Overall, the results provide both mechanistic insight and experimental support for the potential clinical application of the ETV1 inhibitor YK-4-279, highlighting ETS targeting as a promising strategy for osteosarcoma therapy.

Uncontrolled proliferation is a defining characteristic of cancer, making growth suppression a central goal of anticancer therapy. Previous in vivo studies have shown that YK-4-279 can inhibit tumor growth and metastatic spread in prostate cancer xenograft models [44]. In lymphoma systems, it has been reported to suppress malignant cell growth in a concentration-dependent manner [35]. Likewise, melanoma studies have demonstrated that YK-4-279 reduces both survival and proliferative capacity across multiple cell lines, thereby limiting tumor progression [45]. Consistent with these observations, our data confirmed that YK-4-279 significantly impaired OS cell growth and viability, supporting its potential value as an anti-osteosarcoma agent.

Osteosarcoma progression is closely linked to abnormalities in cell cycle control, which depend on the coordinated regulation of cyclins and cyclin-dependent kinases (CDKs) [46]. CDK inhibitory proteins such as p21 and p27 act as negative regulators of cell cycle progression by suppressing cyclin–CDK complex activity, thereby preventing DNA replication and cell cycle transition [47, 48]. Cyclin D1 is widely recognized as an oncogenic regulator involved in cell proliferation and is frequently considered a therapeutic target [49]. Cyclin B, in contrast, is essential for driving cells into mitosis during the G2/M phase [50]. Earlier studies reported that YK-4-279 induces rapid G2/M arrest in Ewing sarcoma cells, associated with reduced Cyclin B1 levels and altered microtubule-associated protein expression, ultimately leading to growth inhibition and apoptosis [51]. In addition, methyl protodioscin has been shown to trigger apoptosis in osteosarcoma cells through caspase-dependent mechanisms and activation of the MAPK pathway [52]. Similarly, Xie DM reported that Tanshinone II A enhances chemosensitivity in osteosarcoma by activating the p38/MAPK pathway, increasing pro-apoptotic proteins such as cleaved caspase-3 and Bax, while suppressing anti-apoptotic markers such as Bcl-2 and caspase-3 [53]. In line with these studies, our results demonstrated that YK-4-279 induced G2/M phase arrest in OS cells, increased p21 and p27 expression, and reduced Cyclin B1 and Cyclin D1 levels. These data indicate that YK-4-279 inhibition of OS cell proliferation is strongly associated with disruption of the G2/M checkpoint.

Many anticancer agents induce DNA damage in rapidly dividing tumor cells by interfering with replication-associated signaling pathways [54, 55]. DNA damage typically activates the upstream kinase ATM and its downstream effector CHK2. Activated ATM subsequently phosphorylates histone H2AX, generating γ-H2AX as a marker of DNA double-strand breaks [56]. In the present study, elevated γ-H2AX foci formation and increased γ-H2AX protein expression were detected in OS cells following YK-4-279 exposure, indicating the occurrence of DNA damage. Once DNA lesions arise, the ATM–CHK2 axis initiates downstream responses, including checkpoint activation, apoptosis, or DNA repair. Our findings further showed enhanced phosphorylation of ATM and CHK2 after YK-4-279 treatment. Collectively, these results indicate that YK-4-279 induces DNA damage signaling, contributing to reduced OS cell viability and proliferative capacity.

The inhibition of tumor cell proliferation is closely linked to the activation of programmed cell death pathways, which represent a central mechanism in anticancer therapy [57]. Accordingly, apoptosis is widely used as a key functional endpoint when evaluating the efficacy of potential anticancer agents. Apoptosis itself is an irreversible and highly coordinated signaling cascade governed primarily by the cysteine protease (caspase) family [58]. Within this system, Caspase 8 serves as an essential initiator of death receptor–mediated apoptotic signaling [59, 60]. Additionally, PARP1 cleavage is routinely recognized as a biochemical indicator of apoptotic progression. The small molecule YK-4-279 has been reported as a potent mitotic disruptor that induces apoptosis across multiple neuroblastoma models with distinct oncogenic drivers [36]. In vivo xenograft studies further demonstrated that YK-4-279 suppresses tumor growth in Ewing sarcoma by disrupting EWS-FLI1 activity and promoting apoptosis [61]. Moreover, combining low-dose docetaxel with YK-4-279 has been shown to intensify apoptotic signaling while concurrently reducing cellular motility and invasive potential in prostate cancer models [62]. In the present work, YK-4-279 significantly increased apoptotic rates in osteosarcoma (OS) cells and enhanced the accumulation of cleaved PARP1 and Caspase 8, consistent with previously reported findings. These results collectively suggest that YK-4-279 may exert anti-OS effects primarily by inducing apoptotic cell death, thereby restricting tumor expansion and progression.

The MAPK (Mitogen-Activated Protein Kinase) signaling network is a fundamental regulator of apoptosis triggered by anticancer interventions. Core MAPK components, including ERK, JNK, and p38, orchestrate essential cellular functions such as proliferation, differentiation, survival, and programmed cell death [63]. Notably, multiple ETS transcription factors are direct downstream targets of MAPK signaling cascades [64, 65].

Therefore, determining whether YK-4-279 modulates this pathway is essential for understanding its mechanism of action in OS. Our findings revealed that YK-4-279 markedly increased phosphorylation levels of ERK1/2, JNK, and p38 MAPK, indicating robust activation of MAPK signaling. Previous evidence has shown that activation of JNK and p38 MAPK can drive apoptosis via G2/M cell cycle arrest [66, 67], which is consistent with our experimental results.

To further confirm the functional role of MAPK signaling in YK-4-279–mediated effects, OS cells were co-treated with YK-4-279 and a p38 MAPK inhibitor to determine whether pathway suppression could reverse its biological activity. The results demonstrated that inhibition of p38 MAPK partially reversed the effects of YK-4-279, leading to decreased apoptosis, partial recovery of DNA stability, and reduced MAPK pathway activation. These observations indicate that YK-4-279 suppresses OS cell survival and proliferation predominantly by activating MAPK signaling, which, in turn, promotes DNA damage, cell cycle arrest, and apoptosis.

YK-4-279 has exhibited broad-spectrum anticancer activity in various tumor types, underscoring its potential as a therapeutic candidate. Our in vitro data in osteosarcoma further support this concept, suggesting strong translational potential for OS therapy. In summary, YK-4-279 suppressed OS cell growth and viability, induced cell cycle arrest, promoted apoptosis, and inhibited tumor progression. These effects are likely mediated through MAPK pathway activation, positioning YK-4-279 as a promising candidate for osteosarcoma treatment.

In addition, in vivo experiments demonstrated that YK-4-279 significantly inhibited tumor growth in an MG63 osteosarcoma xenograft model. This antitumor activity may be associated with activation of DNA damage signaling, as evidenced by elevated γ-H2AX expression, induction of apoptotic pathways indicated by PARP1 cleavage, and stimulation of the p38 MAPK stress response axis. Importantly, administration at an effective dose of 30 mg/kg/day did not produce significant changes in body weight or hepatic and renal biochemical parameters, suggesting that YK-4-279 combines strong in vivo antitumor efficacy with a favorable safety profile.

This work is not without limitations, and further investigations are required to strengthen and extend these findings in several directions. First, future studies should incorporate a larger, more diverse set of osteosarcoma cell lines to better capture tumor heterogeneity and provide a more comprehensive evaluation of the antitumor mechanisms and efficacy of YK-4-279. In parallel, in vivo experimental models should be refined to allow a more detailed and reliable assessment of both therapeutic performance and safety outcomes associated with YK-4-279 administration.

In addition, pharmacokinetic and pharmacodynamic profiling will be necessary to define optimal dosing schedules and to clarify the compound's systemic stability and distribution characteristics. Chemical optimization of YK-4-279 may also be explored to improve solubility, reduce off-target toxicity, and preserve or enhance target specificity. Furthermore, combination therapy approaches involving standard chemotherapeutic agents or immunotherapeutic strategies should be evaluated to determine whether synergistic effects can enhance antitumor activity and help overcome potential resistance mechanisms. Together, these future directions aim to advance the preclinical development of YK-4-279 and support its translation into clinical use.

Conclusion

The present study examined the anticancer effects and underlying molecular mechanisms of YK-4-279 in osteosarcoma (OS). In vitro experiments demonstrated that YK-4-279 markedly reduces OS cell viability and proliferative capacity, induces G2/M arrest, promotes programmed cell death, and causes DNA damage. Mechanistically, these effects were associated with activation of the MAPK signaling cascade, including ERK1/2, JNK, and p38 MAPK, with a pronounced increase in phosphorylation of these signaling components following treatment. Moreover, pharmacological inhibition of p38 MAPK partially counteracted the effects of YK-4-279, highlighting its central role in mediating the observed antitumor responses.

Overall, YK-4-279 exerts its anti-osteosarcoma activity primarily by activating the MAPK pathway, leading to reduced cell survival, cell cycle disruption, DNA damage, and apoptosis. These results support YK-4-279 as a promising candidate for future osteosarcoma therapy.

Acknowledgments: None

Conflict of Interest: None

Financial Support: This study was funded by the Natural Science Foundation of Shandong Province (No. ZR2023QH034).

Ethics Statement: All animal experiments and the use of cell lines in this study were approved by the Medical Ethics Committee of Liaocheng People's Hospital (Approval No. 2022063) and conducted in strict accordance with the NIH Guidelines for the Care and Use of Animals and the principles of the Declaration of Helsinki. The HOS (ZQ0952) and MG63 (ZQ0403) cell lines were purchased from Dr. Zhang Lu at Shanghai Zhong Qiao Xin Zhou Biotechnology Co., Ltd., and authenticated by short tandem repeat (STR) profiling to confirm identity and exclude cross-contamination.

References

1. Moukengue B, Lallier M, Marchandet L, Baud'huin M, Verrecchia F, Ory B, et al. Origin and therapies of osteosarcoma. Cancers. 2022;14(14):3503.
2. Shoaib Z, Fan TM, Irudayaraj JMK. Osteosarcoma mechanobiology and therapeutic targets. Br J Pharmacol. 2022;179(2):201–17.
3. Li J, Gu A, Tang N, Zengin G, Li MY, Liu Y. Patient-derived xenograft models in pan-cancer: from bench to clinic. Interdiscip Med. 2025;3(5):e20250016.
4. Zhao J, Dean DC, Hornicek FJ, Yu X, Duan Z. Emerging next-generation sequencing-based discoveries for targeted osteosarcoma therapy. Cancer Lett. 2020;474:158–67.
5. Chen R, Wang G, Zheng Y, Hua Y, Cai Z. Drug resistance-related microRNAs in osteosarcoma: translating basic evidence into therapeutic strategies. J Cell Mol Med. 2019;23(4):2280–92.
6. Barbosa FAR, Siminski T, Canto RFS, Almeida GM, Mota NSRS, Ourique F, et al. Novel pyrimidinic selenourea induces DNA damage, cell cycle arrest, and apoptosis in human breast carcinoma. Eur J Med Chem. 2018;155:503–15.
7. Hurley LH. DNA and its associated processes as targets for cancer therapy. Nat Rev Cancer. 2002;2(3):188–200.
8. Huang RX, Zhou PK. DNA damage response signaling pathways and targets for radiotherapy sensitization in cancer. Signal Trans Targeted Ther. 2020;5(1):60.
9. Li Z, Pearlman AH, Hsieh P. DNA mismatch repair and the DNA damage response. DNA Repair. 2016;38:94–101.
10. Pawlik TM, Keyomarsi K. Role of cell cycle in mediating sensitivity to radiotherapy. Int J Radiat Oncol Biol Phys. 2004;59(4):928–42.
11. He G, Siddik ZH, Huang Z, Wang R, Koomen J, Kobayashi R, et al. Induction of p21 by p53 following DNA damage inhibits both Cdk4 and Cdk2 activities. Oncogene. 2005;24(18):2929-43.
12. Wang JYJ. Cell death response to DNA damage. Yale J Biol Med. 2019;92(4):771-9.
13. Ishikawa K, Ishii H, Saito T. DNA damage-dependent cell cycle checkpoints and genomic stability. DNA Cell Biol. 2006;25(7):406-11.
14. Angius G, Tomao S, Stati V, Vici P, Bianco V, Tomao F. Prexasertib, a checkpoint kinase inhibitor: from preclinical data to clinical development. Cancer Chemother Pharmacol. 2020;85(1):9-20.
15. Hanahan D, Weinberg RA. Hallmarks of cancer: the next generation. Cell. 2011;144(5):646-74.
16. Huang M, Gong G, Deng Y, Long X, Long W, Liu Q, et al. Crosstalk between cancer cells and the nervous system. Med Adv. 2023;1(3):173-89.
17. Ma P, Wang G, Men K, Li C, Gao N, Li L. Advances in clinical application of nanoparticle-based therapy for cancer treatment: a systematic review. Nano TransMed. 2024;3:100036.
18. Zinn S, Vazquez-Lombardi R, Zimmermann C, Sapra P, Jermutus L, Christ D. Advances in antibody-based therapy in oncology. Nat Cancer. 2023;4(2):165-80.
19. Zhou C, Solomon B, Loong HH, Park K, Pérol M, Arriola E, et al. First-line selpercatinib or chemotherapy and pembrolizumab in RET fusion-positive NSCLC. N Engl J Med. 2023;389(20):1839-50.
20. Tilly H, Morschhauser F, Sehn LH, Friedberg JW, Trněný M, Sharman JP, et al. Polatuzumab vedotin in previously untreated diffuse large B-cell lymphoma. N Engl J Med. 2022;386(4):351-63.

21. Qin S, Chan SL, Gu S, Bai Y, Ren Z, Lin X, et al. Camrelizumab plus rivoceranib versus sorafenib as first-line therapy for unresectable hepatocellular carcinoma (CARES-310): a randomised, open-label, international phase 3 study. Lancet. 2023;402(10408):1133-46.
22. Zhang Y, Zheng WH, Zhou SH, Gu JL, Yu Q, Zhu YZ, et al. Molecular genetics, therapeutics and RET inhibitor resistance for medullary thyroid carcinoma and future perspectives. Cell Commun Signal. 2024;22(1):460.
23. Wang Y, Huang Z, Sun M, Huang W, Xia L. ETS transcription factors: multifaceted players from cancer progression to tumor immunity. Biochim Biophys Acta Rev Cancer. 2023;1878(3):188872.
24. Saulnier O, Guedri-Idjouadiene K, Aynaud MM, Chakraborty A, Bruyr J, Pineau J, et al. ERG transcription factors have a splicing regulatory function involving RBFOX2 that is altered in the EWS-FLI1 oncogenic fusion. Nucleic Acids Res. 2021;49(9):5038-56.
25. Liu Q, Liu Y, Li X, Wang D, Zhang A, Pang J, et al. Perfluoroalkyl substances promote breast cancer progression via ERα and GPER mediated PI3K/Akt and MAPK/Erk signaling pathways. Ecotoxicol Environ Saf. 2023;258:114980.
26. Boone MA, Taslim C, Crow JC, Selich-Anderson J, Byrd RK, Goin-Kochel RP, et al. Identification of a novel FUS/ETV4 fusion and comparative analysis with other Ewing sarcoma fusion proteins. Mol Cancer Res. 2021;19(11):1795-801.
27. Liu Z, Ren Z, Zhang C, Qian R, Wang H, Wang J, et al. ELK3: a new molecular marker for the diagnosis and prognosis of glioma. Front Oncol. 2021;11:608748.
28. Mehtonen J, Teppo S, Lahnalampi M, Kokko A, Kaukonen R, Oksa L, et al. Single cell characterization of B-lymphoid differentiation and leukemic cell states during chemotherapy in ETV6-RUNX1-positive pediatric leukemia identifies drug-targetable transcription factor activities. Genome Med. 2020;12(1):99.
29. Ben-David Y, Gajendran B, Sample KM, Zacksenhaus E. Current insights into the role of Fli-1 in hematopoiesis and malignant transformation. Cell Mol Life Sci. 2022;79(3):163.
30. Hwang SY, Park S, Jo H, Seo SH, Lee D, Kim E, et al. Interrupting specific hydrogen bonds between ELF3 and MED23 as an alternative drug resistance-free strategy for HER2-overexpressing cancers. J Adv Res. 2023;47:173-87.
31. Ma Y, Xu B, Yu J, Zeng X, Shen X, Hu L, et al. Fli-1 activation through targeted promoter activity regulation using a novel 3',5'-diprenylated chalcone inhibits growth and metastasis of prostate cancer cells. Int J Mol Sci. 2020;21(6):2216.
32. Eid W, Abdel-Rehim W. Genome-wide analysis of ETV1 targets: insights into the role of ETV1 in tumor progression. J Cell Biochem. 2019;120(6):8983-91.
33. Wu SP, Cooper BT, Bu F, Bowman CJ, Wang S, Jackson TM, et al. DNA methylation-based classifier for accurate molecular diagnosis of bone sarcomas. JCO Precis Oncol. 2017;2017:PO.17.00031.
34. Erkizan HV, Kong Y, Merchant M, Schlottmann S, Barber-Rotenberg JS, Yuan L, et al. A small molecule blocking oncogenic protein EWS-FLI1 interaction with RNA helicase A inhibits growth of Ewing's sarcoma. Nat Med. 2009;15(7):750-6.
35. Rahim S, Beauchamp EM, Kong Y, Brown ML, Toretsky JA, Üren A. YK-4-279 inhibits ERG and ETV1 mediated prostate cancer cell invasion. PLoS One. 2011;6(4):e19343.
36. Kollareddy M, Zheleva D, Dzubak P, Brahmkshatriya PS, Lepsik M, Hajduch M, et al. The small molecule inhibitor YK-4-279 disrupts mitotic progression of neuroblastoma cells, overcomes drug resistance and synergizes with inhibitors of mitosis. Cancer Lett. 2017;403:74-85.
37. Huang L, Zhai Y, Fajardo CD, Qiu X, Seoane JA, Le AV, et al. YK-4-279 attenuates progression of pre-existing pigmented lesions to nodular melanoma in a mouse model. Cancers (Basel). 2021;14(1):143.
38. Spriano F, Chung EYL, Gaudio E, Tarantelli C, Cascione L, Bouveret M, et al. The ETS inhibitors YK-4-279 and TK-216 are novel antilymphoma agents. Clin Cancer Res. 2019;25(16):5167-76.
39. Liu Z, Zhu Q, Song E, Song Y. Polybrominated diphenyl ethers quinone exhibits neurotoxicity by inducing DNA damage, cell cycle arrest, apoptosis and p53-driven adaptive response in microglia BV2 cells. Toxicology. 2021;457:152807.
40. Saito Y, Zhou H, Kobayashi J. Corrigendum: chromatin modification and NBS1: their relationship in DNA double-strand break repair [Genes Genet. Syst. (2015) 90, p. 195-208]. Genes Genet Syst. 2016;91(4):241.

41. Zhang YY, Feng PP, Wang HF, Zhang H, Liang T, Hao XS, et al. Licochalcone B induces DNA damage, cell cycle arrest, apoptosis, and enhances TRAIL sensitivity in hepatocellular carcinoma cells. Chem Biol Interact. 2022;365:110076.
42. Moruno-Manchón JF, Pérez-Jiménez E, Knecht E. Glucose induces autophagy under starvation conditions by a p38 MAPK-dependent pathway. Biochem J. 2013;449(2):497–506.
43. Notte A, Ninane N, Arnould T, Michiels C. Hypoxia counteracts taxol-induced apoptosis in MDA-MB-231 breast cancer cells: role of autophagy and JNK activation. Cell Death Dis. 2013;4(5):e638.
44. Rahim S, Minas T, Hong SH, Justvig S, Çelik H, Kont YS, et al. A small molecule inhibitor of ETV1, YK-4-279, prevents prostate cancer growth and metastasis in a mouse xenograft model. PLoS One. 2014;9(12):e114260.
45. Huang L, Zhai Y, La J, Lui JW, Moore SPG, Little EC, et al. Targeting Pan-ETS factors inhibits melanoma progression. Cancer Res. 2021;81(8):2071–85.
46. Malumbres M, Barbacid M. Cell cycle, CDKs and cancer: a changing paradigm. Nat Rev Cancer. 2009;9(3):153–66.
47. Torres-Martinez Z, Delgado Y, Ferrer-Acosta Y, Suarez-Arroyo IJ, Joaquín-Ovalle FM, Delinois LJ, et al. Key genes and drug delivery systems to improve the efficiency of chemotherapy. Cancer Drug Resist. 2021;4:163–91.
48. Shamloo B, Usluer S. p21 in cancer research. Cancers. 2019;11(8):1178.
49. Zheng J, Li Q, Wang W, Wang Y, Fu X, Wang W, et al. Apoptosis-related protein-1 acts as a tumor suppressor in cholangiocarcinoma cells by inducing cell cycle arrest via downregulation of cyclin-dependent kinase subunits. Oncol Rep. 2016;35(2):809–16.
50. Fischer M, Müller GA. Cell cycle transcription control: DREAM/MuvB and RB-E2F complexes. Crit Rev Biochem Mol Biol. 2017;52(6):638–62.
51. Zöllner SK, Selvanathan SP, Graham GT, Commins RMT, Hong SH, Moseley E, et al. Inhibition of the oncogenic fusion protein EWS-FLI1 causes G2-M cell cycle arrest and enhanced vincristine sensitivity in Ewing's sarcoma. Sci Signal. 2017;10(499).
52. Tseng SC, Shen TS, Wu CC, Chang IL, Chen HY, Hsieh CP, et al. Methyl protodioscin induces apoptosis in human osteosarcoma cells by caspase-dependent and MAPK signaling pathways. J Agric Food Chem. 2017;65(13):2670–6.
53. Xie DM, Li ZY, Ren BK, et al. Tanshinone II A facilitates chemosensitivity of osteosarcoma cells to cisplatin via activation of p38 MAPK pathway. Chin J Integr Med. 2025;31(4):326–35.
54. Haider T, Tiwari R, Vyas SP, Soni V. Molecular determinants as therapeutic targets in cancer chemotherapy: an update. Pharmacol Ther. 2019;200:85–109.
55. Sadiq Z, Varghese E, Büsselberg D. Cisplatin's dual-effect on the circadian clock triggers proliferation and apoptosis. Neurobiol Sleep Circadian Rhythms. 2020;9:100054.
56. Wang L, Chen J, Li Q, Liu A, Lei Z, Li M, et al. Cigarette smoke extract induces malignant transformation and DNA damage via c-MET phosphorylation in human bronchial epithelial cells. Ecotoxicol Environ Saf. 2024;283:116985.
57. Jiang G, Liu J, Ren B, Zhang L, Owusu L, Liu L, et al. Anti-tumor and chemosensitization effects of cryptotanshinone extracted from Salvia miltiorrhiza Bge. on ovarian cancer cells in vitro. J Ethnopharmacol. 2017;205:33–40.
58. Bai L, Wang S. Targeting apoptosis pathways for new cancer therapeutics. Annu Rev Med. 2014;65(1):139–55.
59. Jiang C, Fang X, Jiang Y, Shen F, Hu Z, Li X, et al. TNF-α induces vascular endothelial cells apoptosis through overexpressing pregnancy induced noncoding RNA in Kawasaki disease model. Int J Biochem Cell Biol. 2016;72:118–24.
60. Wu R, Shen D, Sohun H, Ge D, Chen X, Wang X, et al. miR 186, a serum microRNA, induces endothelial cell apoptosis by targeting SMAD6 in Kawasaki disease. Int J Mol Med. 2018;41(4):1899–908.
61. Minas TZ, Han J, Javaheri T, Hong SH, Schlederer M, Saygideğer-Kont Y, et al. Correction: YK-4-279 effectively antagonizes EWS-FLI1 induced leukemia in a transgenic mouse model. Oncotarget. 2024;15(1):143.
62. Yu L, Wu X, Chen M, Huang H, He Y, Wang H, et al. The effects and mechanism of YK-4-279 in combination with docetaxel on prostate cancer. Int J Med Sci. 2017;14(4):356–66.

63. Nussinov R, Tsai CJ, Jang H, Korcsmáros T, Csermely P. Oncogenic KRAS signaling and YAP1/β-catenin: similar cell cycle control in tumor initiation. Semin Cell Dev Biol. 2016;58:79–85.
64. Charlot C, Dubois-Pot H, Serchov T, Tourrette Y, Wasylyk B. A review of post-translational modifications and subcellular localization of Ets transcription factors: possible connection with cancer and involvement in the hypoxic response. Methods Mol Biol. 2010;647:3–30.
65. Hollenhorst PC, Ferris MW, Hull MA, Chae H, Kim S, Graves BJ. Oncogenic ETS proteins mimic activated RAS/MAPK signaling in prostate cells. Genes Dev. 2011;25(20):2147–57.
66. Liu W, Ning R, Chen RN, Huang XF, Dai QS, Hu JH, et al. Aspafilioside B induces G2/M cell cycle arrest and apoptosis by upregulating H-Ras and N-Ras via ERK and p38 MAPK signaling pathways in human hepatoma HepG2 cells. Mol Carcinog. 2016;55(5):440–57.
67. Thongsom S, Suginta W, Lee KJ, Choe H, Talabnin C. Piperlongumine induces G2/M phase arrest and apoptosis in cholangiocarcinoma cells through the ROS-JNK-ERK signaling pathway. Apoptosis. 2017;22(11):1473–84.